Supporting Online Material for

Cytoplasmic Dynein Moves through Uncoordinated Stepping of the AAA+ Ring Domains

Mark A. DeWitt, Amy Y. Chang, Peter A. Combs, Ahmet Yildiz

Department of Physics, and Department of Molecular and Cellular Biology, University of California, Berkeley, CA 94720, USA.

correspondence to: yildiz@berkeley.edu

This PDF file includes:

Other Supporting Online Material for this manuscript includes the following:

Materials and Methods

Protein Expression, Labeling and Purification

The expression and purification of a native *S. cerevisiae* cytoplasmic dynein motor, tagged with GFP at the N-terminal tail and with DHA (Promega) at the C-terminal head (GFP-Dyn_{471kD}-DHA) was previously achieved (*6*). Non-processive monomers of Dyn_{331kD}, encoding a.a. 1219-4093, were artificially dimerized by fusing their linkers to glutathione s-transferase (GST) at the N-terminus (*6*). *In vitro* motility assays demonstrated that GFP-GST-Dyn_{331kD} moves processively with a similar speed to that of full-length dynein (*6*). To specifically label dynein with fluorophores or biotin, a 26kDA DHA domain (Promega) was genetically encoded at either the C-terminal head domain or the N-terminal tail domain (*6*). Heterodimeric dynein mutants were prepared by replacing the N-terminal GST tag with FRB and FKBP12 domains that dimerize in the presence of rapamycin (*24*). Monomeric dynein bearing a single point mutation (Mut_h, a glutamic acid to a glutamine point mutation (E1849Q) in the Walker B motif of AAA1) (*2, 16*) was a generous gift of R.D. Vale.

All dynein constructs were purified using IgG beads and TEV protease cleavage, as described previously (*6*). For one-color tracking assays, the homodimeric Dyn_{331kD} constructs were labeled with 10 μM HaloTag-biotin during protein purification. The excess ligand was removed while the dynein was attached to the IgG sepharose affinity column. The FKBP12-Dyn_{331kD}-DHA monomer (WT_h) was prepared by labeling with 10 μM HaloTag biotin as well. The FRB-$AAA1_{E/Q}Dyn_{331kD}$-DHA monomer (Mut_h) was prepared without any labeling.

Microscope

An objective-type total internal reflection fluorescence (TIRF) microscope was set up, using a Nikon Ti-E Eclipse inverted fluorescence microscope equipped with a perfect focusing system and 100X 1.49 N.A. Plano Apo oil immersion TIRF objective (Nikon). A 488 nm diode-pumped solid-state laser (Coherent Sapphire, 500 mW) was used for quantum dot (QD) and GFP excitation. In two-color experiments, QD-585 and QD-655 fluorescence was split into two channels (Q630LP dichroic mirror, Chroma) and imaged separately on the same CCD chip using an Optosplit II image splitter (Cairn Instruments). QD-585 and QD-655 signals were filtered through 585/40 and 655/40 bandpass emission filters (Semrock), respectively, to reduce crosstalk between the two fluorescent channels to below 1%. One-color tracking measurements were recorded with a fast acquisition electron-multiplied charge-coupled device (EM-CCD) camera (Ixon EM^+, 128x128 pixels, Andor Technology) with an effective pixel size of 160 nm after magnification. Two-color data were collected with a 512x512 pixel EM-CCD camera (Andor Technology) with an effective pixel size of 106 nm.

One-Color QD Labeling and Motility Assays

One-color motility assays were performed on sea urchin axonemes (*25*) non-specifically adsorbed to glass coverslips. The glass surface was then pre-blocked with 1 mg/mL

casein in dynein assay buffer (DLB; 80 mM HEPES pH 7.4, 1 mM EGTA and 2 mM $MgCl_2$, 10% glycerol). Biotinylated GFP-GST-Dyn_{331kD}-DHA was flowed in at ~1 nM concentration to sparsely coat axonemes (determined by imaging the GFP fluorescence). After 1 minute, unbound motors were washed with 40 µl DLB buffer containing 1 mg/ml casein. Streptavidin-coated QD-655s were flowed in at 200 nM concentration and reacted with dynein for 2 minutes. Dynein motors were labeled after they were attached to axonemes to prevent aggregation on multivalent QD probes. Comparison of the number of GFP spots versus QD spots on axonemes in separate fluorescent channels showed that ~10% of dynein molecules are labeled with a QD under these conditions (data not shown). Streptavidin-QD labeling was highly specific as we did not observe any binding of QD to non-biotinylated dynein motors in motility assays (data not shown). The sample was imaged in the presence of DLB containing 5-12 µM ATP, 1 mg/ml casein, an ATP regeneration system (2 mM phosphoenolpyruvate and 0.1 mg/ml pyruvate kinase, (1)). 2% β-mercaptoethanol was also added to reduce QD blinking (*26*). To clearly identify dynein stepping in one-color assays, temporal resolution of image acquisition was increased to 2 msec while retaining nanometer localization. Labeling dynein with a QD did not substantially affect the motile properties of the motor based on motor run lengths and velocities (*6*).

Two-Color QD Labeling

For two-color tracking measurements, homodimeric motors (GST-Dyn_{331kD}-DHA or GFP-Dyn_{471kD}-DHA) were labeled with HaloTag-coated QDs, which are significantly smaller than commercially available streptavidin-coated QDs (Table S1). Amino-coated QD-655 and QD-585 (Invitrogen) were reacted with HaloTag-SEO4 ligand (Promega) at ~1000-fold excess for 2-4 hours at room temperature in DLB buffer. The reaction was quenched by addition of 20 mM Tris pH 7.4 (15 min), and the from free label was removed using 20 KDa molecular weight cut-off spin concentrators four times prior to labeling. 50 nM dynein motors were reacted for 15 minutes with a mixture of excess (1-5 µM) HaloTag-coated QD-585 and QD-655 prior to introduction to the flow chamber. HaloTag-coated QD labeling was highly specific to the DHA domain inserted at the C-terminus of the motor, as we did not observe binding of these QDs to dynein without a DHA domain (data not shown). Since the observed dual-labeling efficiency was < 10% for microtubule-bound dynein motors in the presence of excess QD, no crosslinked aggregates were expected under these conditions. Furthermore, fluorescence images of both QDs exhibited complete blinking and uniform intensity in each fluorescent channel, strongly indicating that single QD-585 and QD-655 were attached to the dimer.

For the WT_h/Mut_h heterodimer experiments, WT_h was labeled with biotinylated HaloTag ligand during the purification step. The heterodimer was first constructed by a mixture of equimolar (1 µL each of 50 nM) amounts of WT_h-biotin and unlabeled Mut_h in the presence of 200 nM rapamycin for 10 minutes, prior to labeling with QDs (*6*). 100 nM rapamycin was maintained in all solutions. To rule out the possibility that the experiment may select a small fraction of homodimers that might form in the sample, we verified that processive movement was not observed when only FRB- or FKBP12-tagged motors were introduced to the flow chamber. The mixture of FRB- and FKBP12-tagged motors started to move processively after Rapamycin addition. In addition, different labeling

chemistries were used to attach different colors of QDs to FRB- and FKBP12-tagged dynein monomers. Mut_h and WT_h-biotin were labeled specifically with 100-fold excess of HaloTag-coated QD-585 and streptavidin-coated QD-655, respectively. The reaction with the QDs was allowed to proceed for 15 minutes. Biotin was added to 1mM to the motor-QD mixture immediately prior to addition to sample chamber to prevent surface attachment of streptavidin-coated QDs to biotin-BSA.

Two-Color Motility Assays

Two-color tracking assays were performed on surface-immobilized microtubules. The coverslips were coated with 1 mg/ml biotin-BSA and then treated with 1 mg/ml streptavidin. Porcine tubulin (1:20 of biotin-tubulin to unconjugated tubulin) was polymerized in the presence of 10 μM taxol in BRB80 buffer (80 mM PIPES, 1mM $MgCl_2$ 1mM EDTA, 10% glycerol, pH 6.8) (*27*) and immobilized onto the streptavidin-coated flow chamber. Unbound microtubules were washed off with excess BRB80 buffer. Dynein-QD complexes were flowed onto the microtubules in DLB containing 1 mg/ml casein.

For the homodimeric dynein experiments, moving dyneins were imaged in the presence of 7 μM ATP, 20 mM phosphoenolpyruvate, 0.1 mg/mL pyruvate kinase (Roche), and 1% β-mercaptoethanol. Movies of dual-labeled dyneins were acquired at 30 msec temporal resolution (k_{step} = 0.06 steps/frame). For the heterodimeric dynein experiments, images were acquired at 15 msec temporal resolution in the presence of 40 μM ATP (k_{step} = 0.07 steps/frame). Dual-labeled moving spots were further analyzed for step size measurements.

Image Registration

To precisely measure the relative positions of QD-585 and QD-655, the two fluorescence channels were registered with respect to each other. Potential sources of error in these measurements include the positional offset, rotational and magnification differences between the two channels, irregularities in the CCD chip (*28*), local spherical aberrations in the optical system and chromatic aberrations (*11*). Chromatic aberrations can be corrected if the same (or isospectral) set of probes are used in image registration and data collection. The relative distortions between the two channels were corrected using custom routines implemented in LabVIEW (National Instruments), MATLAB (The Mathworks), and Python using the SciPy package. A metallic film sample decorated with 180 nm nanoholes was translated in 20 nm increments in x and y axes by a piezoelectric nanopositioner (P527.3CD, Physik Instruments), ensuring subpixel coverage of the entire CCD surface. In a separate experiment, the sample was moved randomly in the *xy* plane by a micropositioning stage (MicroStage-20E Mad City Labs) for 5000 frames to achieve coverage of the CCD surface and similar results were obtained. The sample was imaged under brightfield illumination synchronously with translation using custom image acquisition software written in LabVIEW. These images were processed to map the spot centers (0.8 nm localization accuracy) of the nanoholes from one half of the CCD to the other. Fig. S3 shows that the two fluorescent channels were registered with an average error of 2.53 nm. Second order corrections were determined by imaging and localizing custom-made dual-labeled fluorescent probes to avoid chromatic aberration.

For Cy3 and Cy5 imaging assays, 100 µl of 0.2% (weight/volume) 200-nm diameter non-fluorescent amino polystyrene beads (Invitrogen) were labeled with a mixture of 10 µl of 4 mM Cy3 and 4 mM Cy5 NHS-ester. The brightness of these beads were >100 fold higher than that of single Cy3 and Cy5 probes, indicating that each bead is coated with hundreds of fluorescent dyes (data now shown). Coverslips were sparsely decorated with surface-immobilized Cy3/Cy5 beads. As a control, we scanned the CCD chip for 10 microns either in the horizontal or vertical directions, by taking 100 nm steps with a motorized stage (MadCity Labs, Microstage 20E). Matching fluorescent spots in Cy3 and Cy5 channels were fit to a 2D Gaussian. The two channels were registered to ~ 5 nm precision using a different set of Cy3/Cy5 beads within the same sample. Localization and calculation of offsets were performed using MATLAB and Python. The position of a single bead in Cy3 and Cy5 channels colocalize to within 0-4 nm in both x and y directions throughout the entire scan. The fluctuations in distance measurements were in the range of 6-8 nm, largely due to the localization error. These measurements were repeated using a different set of beads (scans 1-13) at different locations and directions on the CCD surface to verify that the mapping technique can reliably measure the distance between the two fluorophores throughout the entire CCD chip.

We have also tested our ability to measure the distance between Cy3 and Cy5 dye molecules using our mapping method (Fig. S3D). 57 bp duplex DNA, labeled with Cy3 and Cy5 dyes on each of the 5' ends was purchased (IDT DNA). 5 nM DNA was non-specifically attached to a glass coverslip coated with 1 mg/ml polylysine in TE buffer with magnesium (10 mM Tris, 1 mM EDTA, 1 mM $MgCl_2$, pH 7.50). The surface was washed with 100 µL of TE with magnesium. The dual-labeled oligonucleotides were excited with 633 and 532 nm lasers and imaged at 500 msec temporal resolution. The two fluorescent channels were registered as described above. Localization error for each Cy3-Cy5 pair were calculated separately and only the pairs localized within 5 nm standard error of the mean were included in the data analysis.

For QD-585 and QD-655 imaging assays, QD-655 amino were coated with excess of Rhodamine Red-X NHS-ester (Invitrogen), which is iso-spectral to QD585 in 550-610 nm bandwith of the emission filter. The QD655-RhodamineX probes were used as a fiducial marker that appears in both QD585 and QD655 channels, which can be registered with 3 nm accuracy. Single dual-QD labeled DNA complexes were scanned across large areas on the CCD surface to test whether large variations in distance measurements between different QD-DNA complexes is due to poor image registration in parts of the CCD surface. Individual dual-QD DNA complexes with significantly different mean inter-QD distance, were selected and scanned at different parts of the CCD. The standard deviation of the magnitude of the inter-QD vector (r) of a single QD-DNA complex was 7-10 nm, which is significantly lower than the 18 nm standard deviation of distance measurements of 50 QD-DNA molecules. The angle of the inter-QD separation to horizontal was also highly conserved during the scan, the standard deviation of the angle of the vector was within 10-20°.

We have performed distance measurements of single DNA polymers labeled with QD585 on one end and QD655 at the other end. The expected length of the DNA polymer is 18.3 nm. The diameters of QD probes were measured as 17 nm and 21 nm, respectively (Table S1). Therefore, we expect the center-to-center distance between the two QDs to be ~37 nm, assuming that central locations of QDs is along the same line with DNA. The average end-to-end distance of dual QD labeled DNA molecules was 34 ± 18 nm (fig. S5B).

Step Size Analysis

The QD position was determined by Fluorescence Imaging with One Nanometer Accuracy (FIONA) (*7*), using a two-dimensional Gaussian fitting algorithm in MATLAB. The standard deviation of the center of the Gaussian fit, which represents the position of the QD center when dynein motors dwell between steps varied. The average error was 4 nm for the homodimer and 4.4 nm for the WT_h/Mut_h heterodimer. These fluctuations were higher than that of surface immobilized QDs 1-3 nm (st. dev.) under the same experimental and imaging conditions. Therefore, the experimental noise in our assay is mostly inherent to the fluctuation of the dynein motor on microtubules, rather than photon shot noise.

The one-color traces were fit using a step finding algorithm (*29*), using a least-squares minimization. All of the analyzed traces were visually examined for the goodness of the fit. Minimum detectable step size was set to 3 nm. Typically, more than 20 steps can be detected from a single run. The two-color traces were fit in a two-dimensional plane (significant deviation in either axis constitutes a step) (*20*). To ensure our ability to detect individual steps taken by dynein in two-color tracking assays (7 μM ATP, 30 ms temporal resolution), we have compared the two color step sizes with that of one-color measurements performed at ~10 fold faster image acquisition rate per dynein step (5-12 μM ATP, 2 ms per frame, Figure 1). Average forward step sizes of one-color (10.6 nm) and two-color WT homodimer (12.0 nm) measurements are in good agreement with each other.

Interhead Distance Measurements

To reliably measure interhead separation of a dynein dimer, we used organic dyes (~1 nm across), which are significantly smaller than QDs. GST-Dyn_{331kD}-DHA dynein was labeled for 30 minutes with a mixture of Cy5-HaloTag and Cy3-HaloTag reagent. The Cy3- and Cy5-HaloTag reagent was prepared by reaction of a 1 mM Cy3- or Cy5-NHS ester (GE Healthcare) with 100 μM HaloTag-SEO4 reagent (Promega) for 2 hours, followed by quenching with 10 mM Tris, pH 8.0. The labeled dynein was flowed onto surface-immobilized microtubules. 1 mM ATP was added for 10-30 sec to allow dynein to adopt a relevant stepping conformation. Under these conditions, we observed > 90% of the motors moving processively along microtubules (data not shown). The flow chamber was then washed with 200 μl DLB to remove ATP and free label. 1 mM AMP-PNP (a non hydrolysable ATP analogue) was then flowed in to tightly attach motors to the microtubules (*13*). Static dynein motors were imaged by 532 and 633 nm laser excitation (Coherent Inc.) in TIRF mode. Each spot was localized and mapped using the software and equipment described above. To exclude dynein motors that are nonspecifically

adhered to the glass surface, we have only analyzed microtubules that are labeled with four or more labeled dynein motors.

In dynein interhead separation measurements, we calculated the average position of each head per dwell location. Since the average dwell time of dynein was equivalent to acquisition of 10 frames in our imaging conditions, standard error of the mean per QD position was on average 1.4 nm. Therefore, we estimated that the error in interhead separation measurements was ~3.7 nm, which includes both the localization errors of the QDs and the registration error.

Dynamic Light Scattering Measurements

Dynamic light scattering (DLS) measurements of QD size were conducted on a Malvern Zetasizer Nano. QDs were diluted to 20-40 nM in PBS (10 mM sodium phosphate pH 7.4, 137 mM NaCl, 3 mM KCl) and filtered through a 0.2 μm syringe filter immediately prior to measurement. The count rates were typically in the range of 150-300 kcps. Five consecutive runs of 3 minutes were averaged for each experiment and three experiments were conducted for each QD sample. Data were fit by volume weighting using the built-in software. The sizes are reported in Table S1.

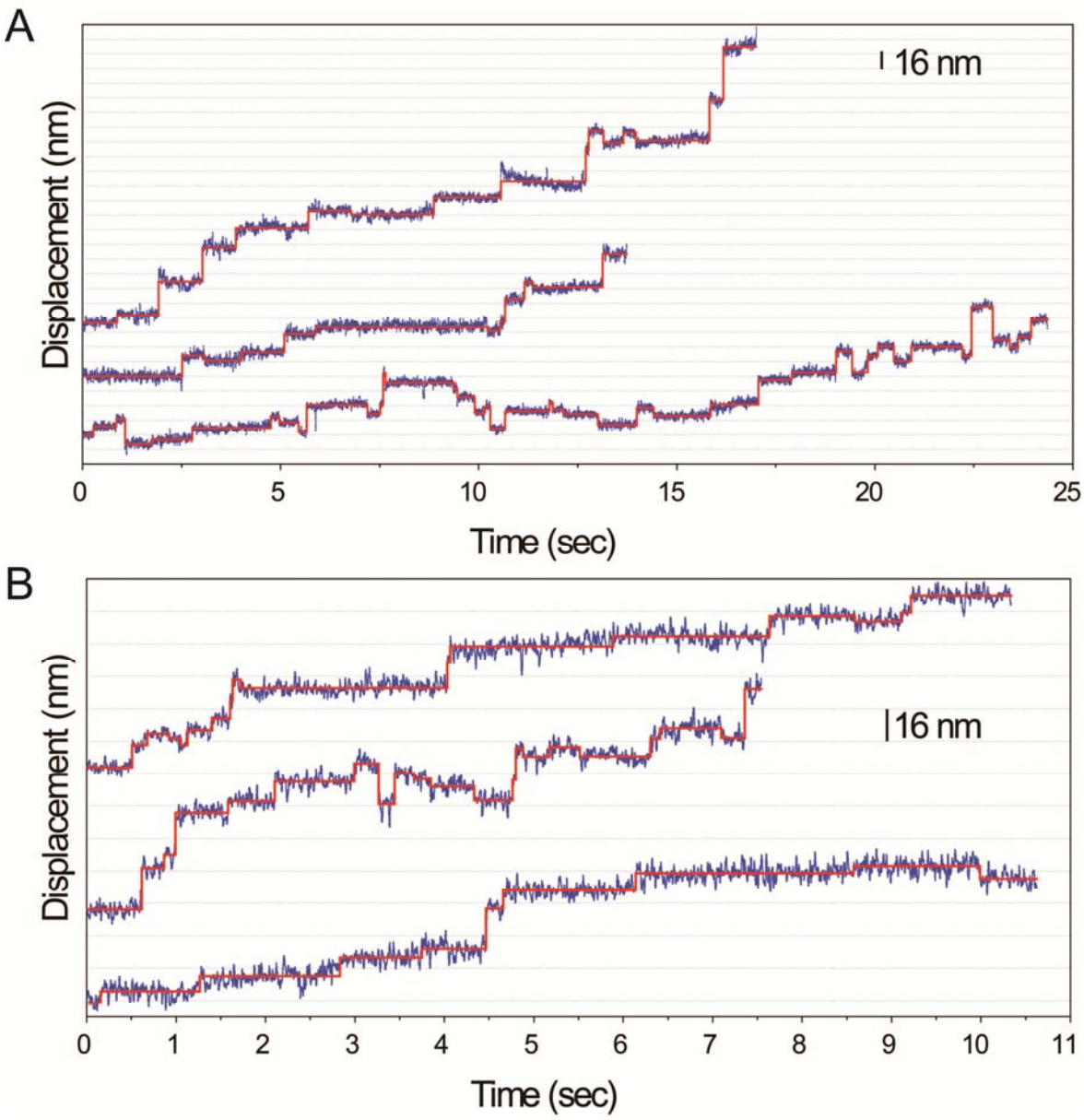

Figure S1. Additional stepping traces of GST-Dyn$_{331kD}$ motors labeled with a single QD-655. A streptavidin-coated QD-655 was localized at 2 msec temporal resolution in the presence of 12 μM ATP. (**A**) Traces of head-labeled dynein. (**B**) Traces of tail-labeled dynein. See Fig. 1 for details.

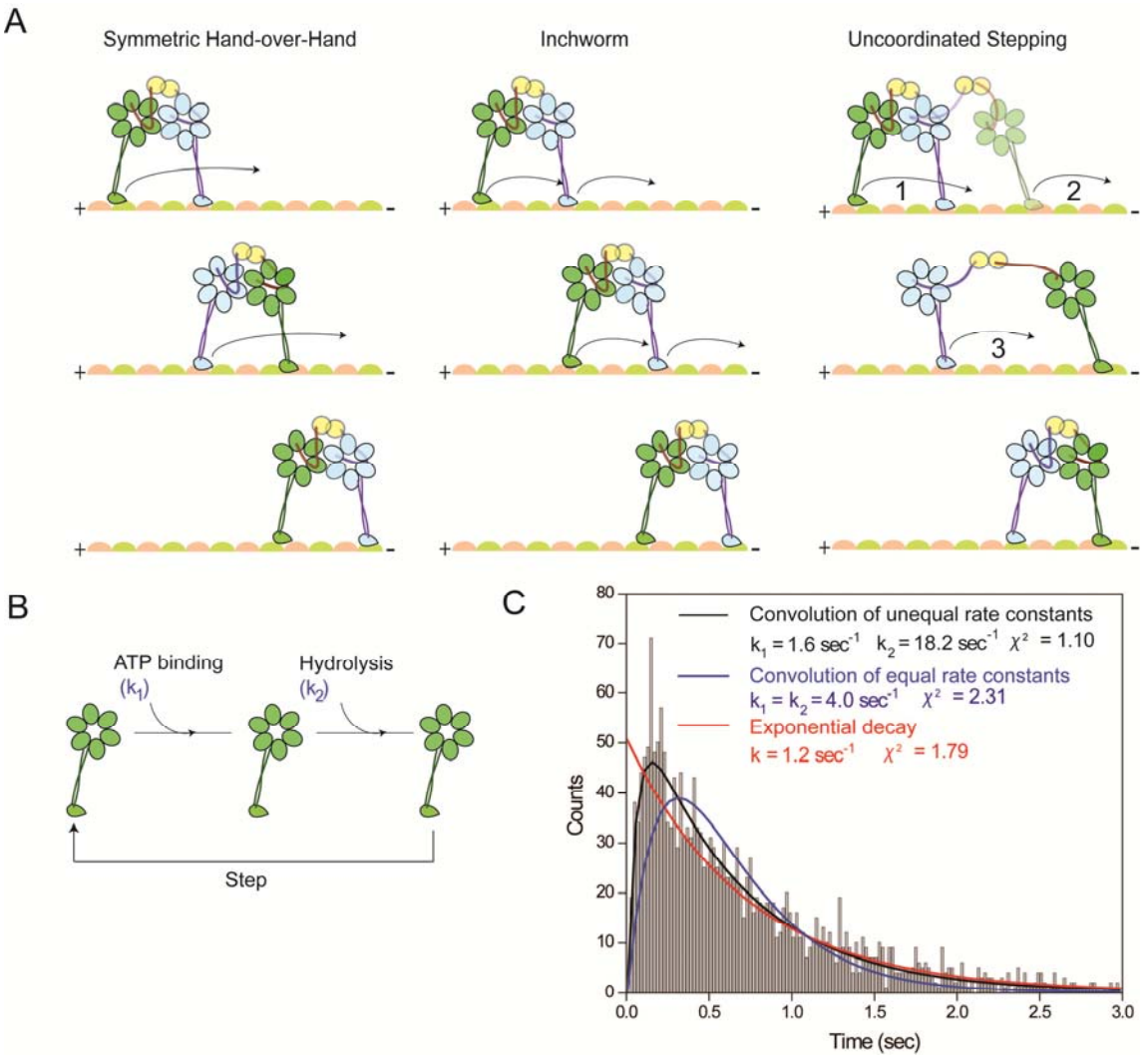

Figure S2. (A) Possible models for dynein processivity. In a symmetric hand-over-hand model, the two heads (green and blue) alternately take steps and exchange the lead position. Each head moves once for every other step of the motor, and the tail moves half the head step size for every step of the motor. If there is a single rate-limiting constant for a head to take a step, the model predicts the stepping kinetics of an individual head to be a convolution of two equal rate constants. In the inchworm model, both heads move together at every step of the motor and the heads do not exchange leads. The tail step size is equal to that of the head. The model predicts the stepping kinetics of an individual head to be a single exponential decay. In the uncoordinated stepping model, the heads do not strictly follow either of the hand-over-hand or inchworm models. Instead, either head is equally likely to take a step. The tail still moves half the head step size when either of the heads take a step. This model predicts the kinetics of both head and tail stepping to fit to a single exponential decay. **(B)** Dynein stepping requires the binding and hydrolysis of ATP at the catalytic (head) domain. At low (< 10 μM) ATP concentrations, ATP binding becomes rate-limiting. At saturating (> 1 mM) ATP concentrations, the motor will be limited by the ATP turnover rate. At intermediate ATP concentrations, then the dwell time distribution of a head would be a convolution of two unequal rate constants,

assuming that dynein walks inchworm or in an uncoordinated manner. In contrast, if dynein walks hand-over-hand, the dwell time distribution would be best fit by a convolution of two identical (uncoordinated) heads, each stepping via a convolution of two unequal rate constants. (**C**) A histogram of dwell times between the steps of head-labeled GST-Dyn_{331kD} at 12 μM ATP (N_{dwells} = 1952). Data were fit to a convolution of two unequal exponential rate constants ($y = A*[exp^{-k1t} - exp^{-k2t}]$, black curve), a convolution of two equal exponential rate constants ($y = A*t*exp^{-kt}$, blue curve) and to a single exponential decay ($y = A*exp^{-kt}$, red curve). Out of the three functions, only the convolution of two unequal exponential rate constants produces a good fit (χ^2 = 1.10) to the histogram. The slow rate (k_1 = 1.59 sec^{-1}) may correspond to ATP binding and the fast rate (k_2 = 18.3 sec^{-1}) may correspond to the ATP turnover rate. k_2 is in close agreement with the previously reported catalytic rate (k_{cat} = 16.1 ± 0.3 ATP/dimer/s) for yeast cytoplasmic dynein, as measured in bulk microtubule-stimulated ATPase assays (*6*).

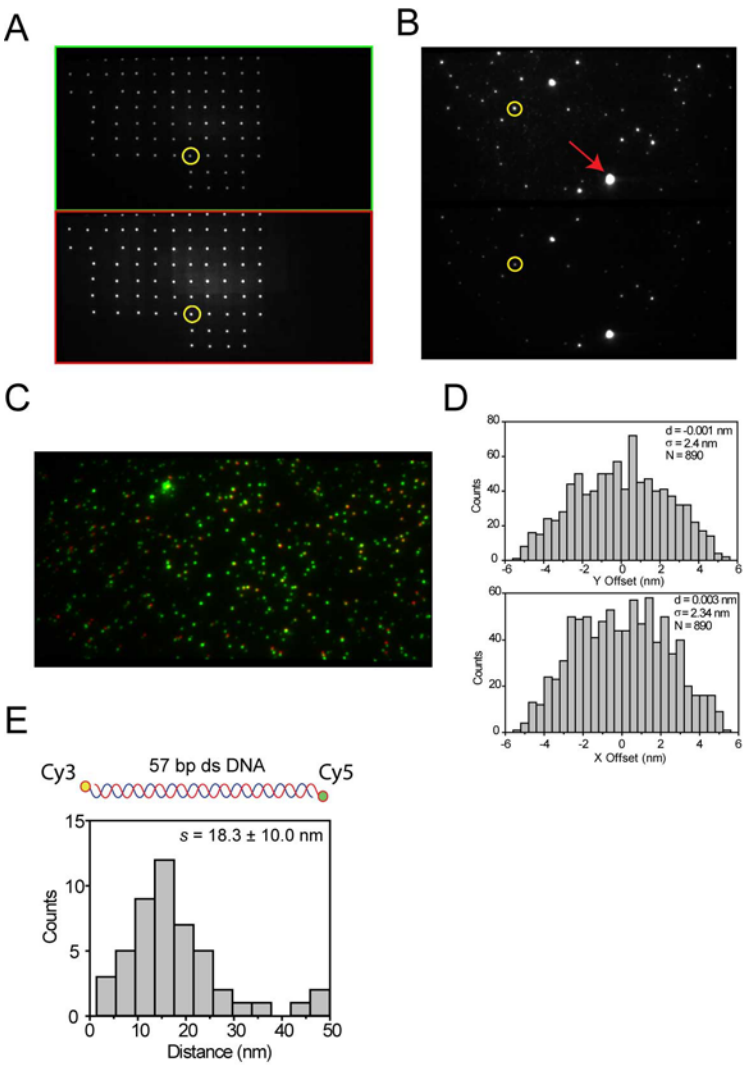

Figure S3. Registration of the two fluorescent channels. (**A**) A metallic film decorated with 180 nm diameter nanoholes was imaged under brightfield. Pairs of matching nanohole images (yellow circles) in two channels of the CCD were automatically detected and their positions were determined by two-dimensional Gaussian fitting for the first round of calibration. The sample was scanned with 20 nm increments in the *xy* plane to achieve sub-pixel registry in the entire CCD surface. (**B**) Pairs of Cy3/Cy5 fluorescent beads (yellow circles) were detected by using the calibration data obtained from nanohole imaging. A second round of calibration using a Cy3/Cy5 bead image was performed to refine the mapping algorithm. Aggregates (red arrow) in the sample were excluded from analysis. (**C**) Pairs of QD655 (green)/Rhodamine Red-X (red) probes were colocalized to correct the chromatic aberrations between QD655-QD585 channels. (**D**) Histogram of registration error between 890 individual QD655/Rhodamine Red-X pairs shows that the two channels can be registered together with an average error of 2.4 nm, in either direction. (**E**) 57 bp duplex DNA was labeled with Cy3 and Cy5 dyes at opposite ends. The two fluorescent channels were registered using an image registration map. The distance between Cy3 and Cy5 was measured to be 18.3 ± 10.0 nm (mean ± st.dev.)

which agrees well with the expected length of the DNA molecule (18.8 nm).

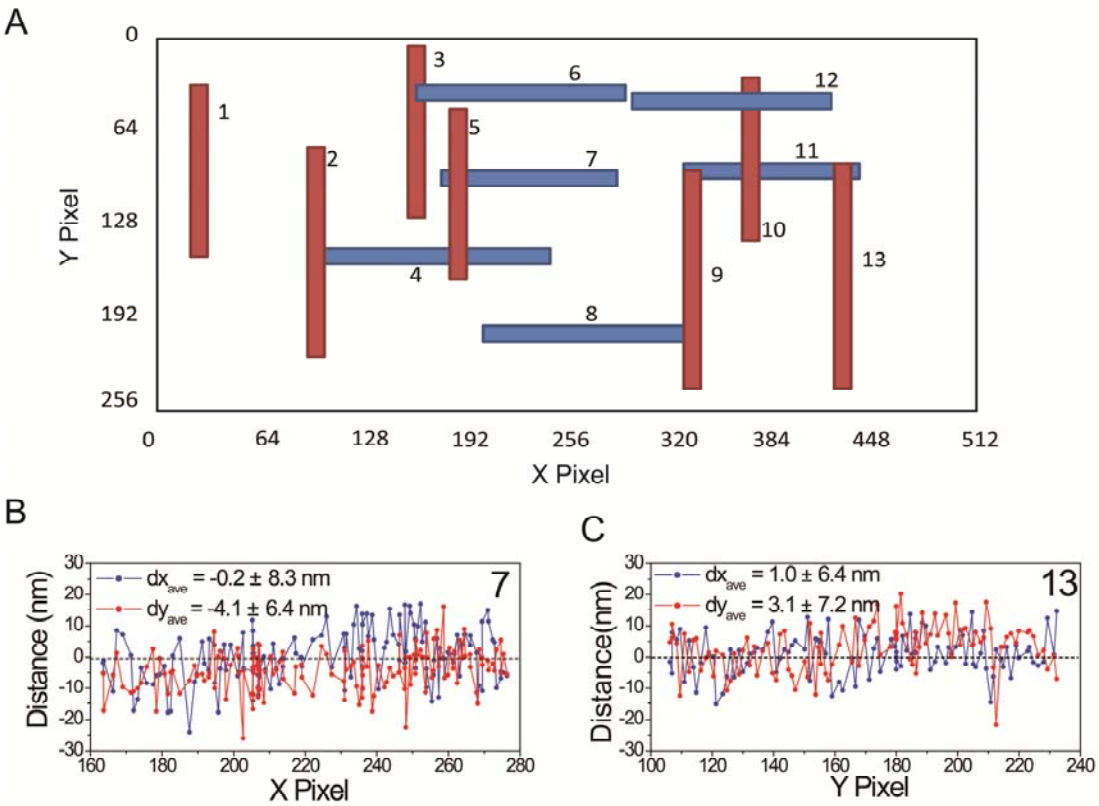

Figure S4. (**A**) Surface-immobilized Cy3/Cy5 beads were scanned in 100 nm increments along the CCD surface for ~10 microns either in the horizontal or vertical direction. The distances between the positions of the bead in the Cy3 and Cy5 channels were calculated using the image registration algorithm. (**B-C**) Examples of a horizontally (spot #7) and vertically (spot #13) scanned beads. Measured distances in x (blue dots) and y (red dots) directions were plotted at each pixel position of the bead. Both Cy3 and Cy5 dyes colocalize well to within 0-4 nm in both x and y directions throughout the entire scan. The fluctuations in distance measurements are in the range of 6-8 nm, due to the localization error. These measurements were repeated using different set of beads (scans 1-13) at different locations and directions on the CCD surface to verify that the mapping technique can reliably measure the distance between the two fluorophores throughout the entire CCD chip. For all of the 13 scanned beads, the average distance in x and y directions was 1.8 nm and 0.1 nm, respectively.

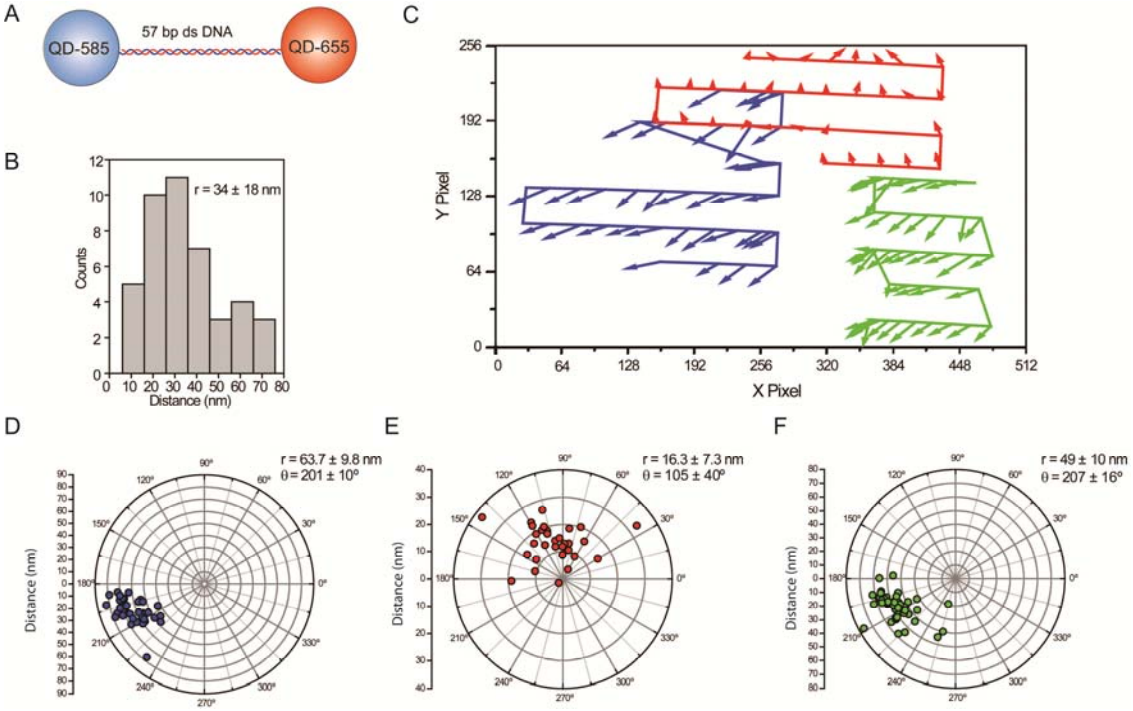

Figure S5. (A) 57 bp duplex DNA was labeled with QD585 and QD655 streptavidin at the opposite ends. (**B**) The fluorescent images were registered using the mapping algorithm using QD655 coated with excess Rhodamine Red-X as a fiducial marker. The distance between the center of the two QDs was measured as 34 ± 18 nm (mean ± st.dev.), which is significantly larger than the expected length of the DNA molecule (18.8 nm) due to the large size of the QD probes (Table S1). (**C**) Individual dual-QD labeled DNA complexes were scanned across large areas on the CCD surface to test whether large variation in distance measurements between different QD-DNA complexes is due to poor image registration in parts of the CCD surface. (**D-F**) The polar plot of the inter-QD separation vector for three independent scans with significantly different mean inter-QD distances. The standard deviation of the magnitude of the inter-QD vector (*r*) of a single QD-DNA complex was 7-10 nm, which is significantly lower than the 18 nm standard deviation of distance measurements of 50 different QD-DNA molecules. The fluctuations of the angle of the inter-QD separation vector to the horizontal were also limited to 10-20°, showing that both the magnitude and the orientation of the inter-QD separation vector can be measured with high precision. When the inter-QD distance was lower than 20 nm, the variation in angle measurements were increased to 30-40° (see an example in E), because localization and registration errors are no longer negligible at short distances.

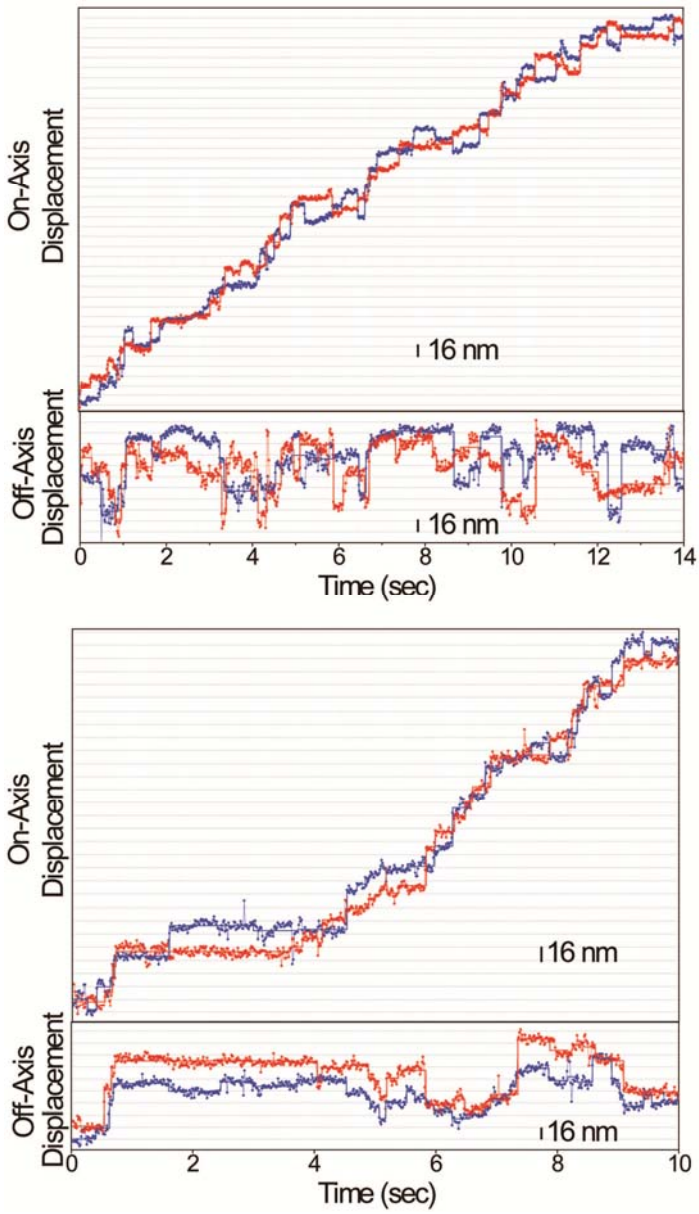

Figure S6. Additional examples of the stepping motion of dual-labeled GST-Dyn$_{331kD}$ motors, including off-axis stepping. Blue and red traces represent positions of QD-585 and QD-655, respectively, as dynein moves along the microtubule. The two heads can also step independently in the off-axis, and remain well-separated during the entire processive run. The heads show no bias to step towards right or left directions along the microtubule off-axis. Lateral stepping of dynein shows no clear preference of helical motion in either direction over the course of > 1 μm movement along the microtubule long axis.

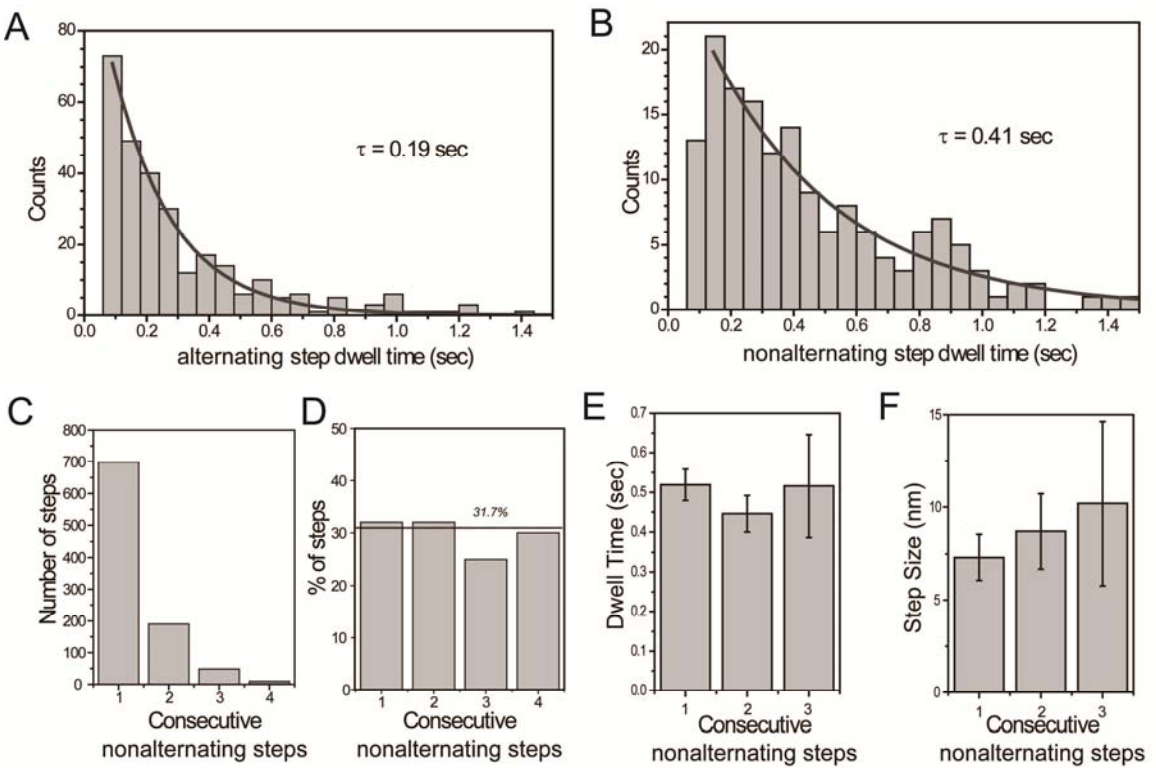

Figure S7. (**A)** Histogram of dwell times between the alternating-head steps of GST-Dyn_{331kD}. Data fits well (R^2 = 0.97) to a single exponential (black line) with a decay constant of 0.19 ± 0.01 sec/step. (**B)** Histogram of dwell times between consecutive steps taken by the same head (nonalternating steps), before the other head takes a step (exponential decay constant: 0.41 ± 0.03 sec/step, R^2 = 0.94). The ~2-fold difference between the stepping rates of nonalternating and alternating steps favors alternating stepping of the heads. (**C**) Number of steps observed for 1-4 consecutive nonalternating stepping events. (**D**) The probability of nonalternating stepping, after 0-3 consecutive nonalternating steps remains constant and agrees well with the probability calculated from the decay constants of alternating and nonalternating steps (31.7%). Due to the finite temporal resolution of the experiment, stepping of the heads occurring within one data point of each other was excluded from data analysis. (**D-E**) The average dwell time and step size of 1-3 consecutive steps (mean ± s.e.m.), respectively.

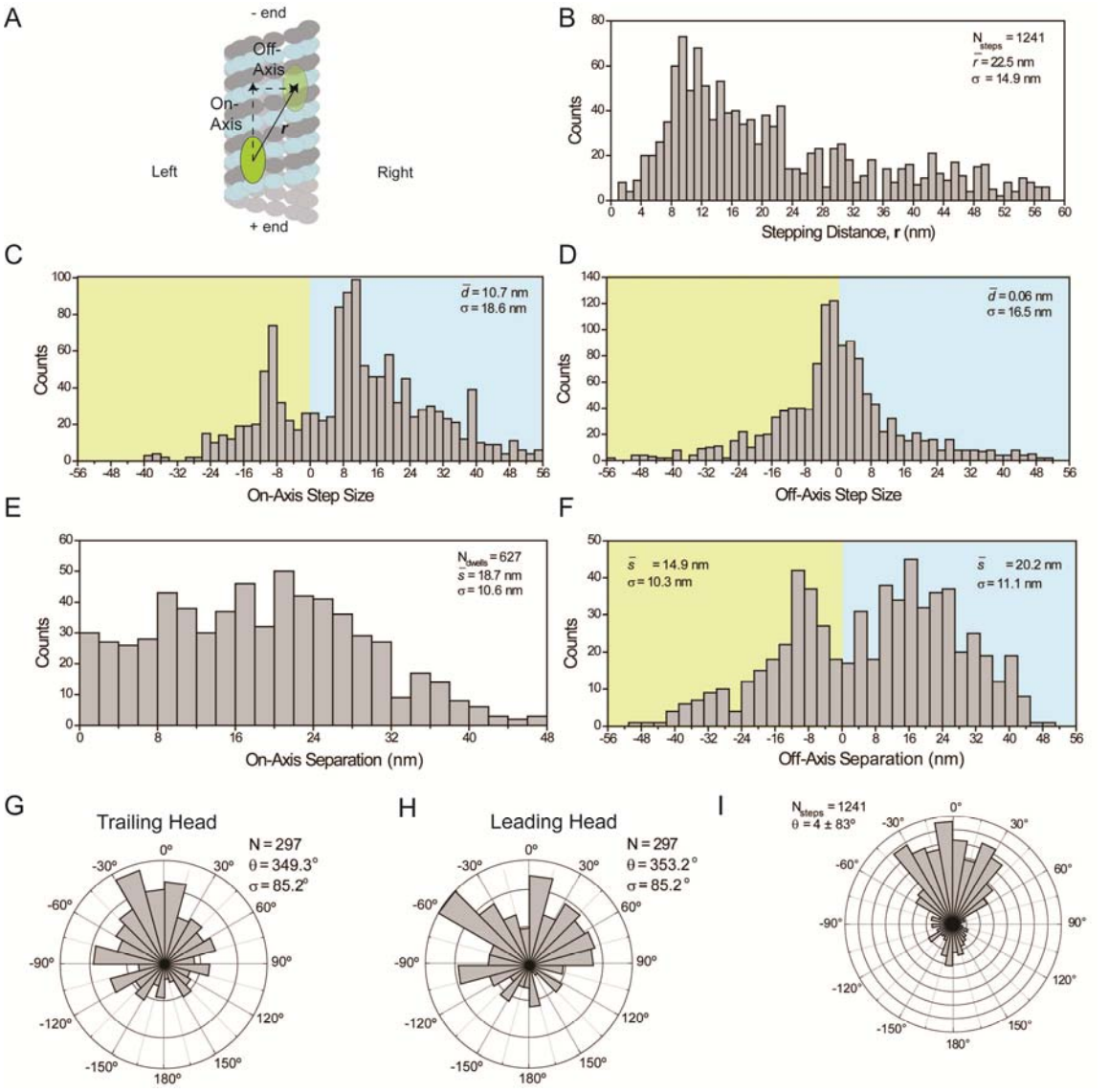

Figure S8. Detailed analysis of the stepping characteristics and interhead orientation of dual-labeled of GST-Dyn$_{331kD}$ motors during processive runs. (**A**) A microtubule diagram shows two dimensional step analysis of a dynein head (green ellipse). Vector summation of on-axis and off-axis step sizes results in a stepping vector (***r***) of the head. (**B**) Histogram for the stepping distance (magnitude of ***r***) is broadly distributed (22.5 ± 14.9 nm, mean ± st.dev, N = 1241). (**C**) Histogram of on-axis head step sizes. The average step size, d = 10.7 nm is similar to that of the one-color step size histogram shown in Figure 1C (d = 10.6 nm). (**D**) Histogram of off-axis head step sizes. Dynein heads can take >20 nm lateral steps without a net bias towards the right (blue area) and left (yellow area) directions (d = 0.06 nm). (**E**) Histogram of the on-axis separation between the trailing and leading head positions during the dwell periods. Average on-axis separation between the heads, s, is 18.7 ± 10.6 nm (mean ± st. dev., N = 627) (**F**) Histogram of off-axis separation between the trailing and leading heads. On average, QD-585 labeled head is separated by 20.2 ± 11.1 nm to the right (blue shaded area) and 14.9 ± 10.3 nm to the left (yellow shaded area) of the QD-655 labeled head. (**G-H**) Histograms of the angle (θ) between stepping and interhead separation vectors for the trailing and the leading heads,

respectively. (**I**) Histogram of the stepping angles of a head with respect to the microtubule minus end. 0° corresponds to an axis parallel to the microtubule minus end.

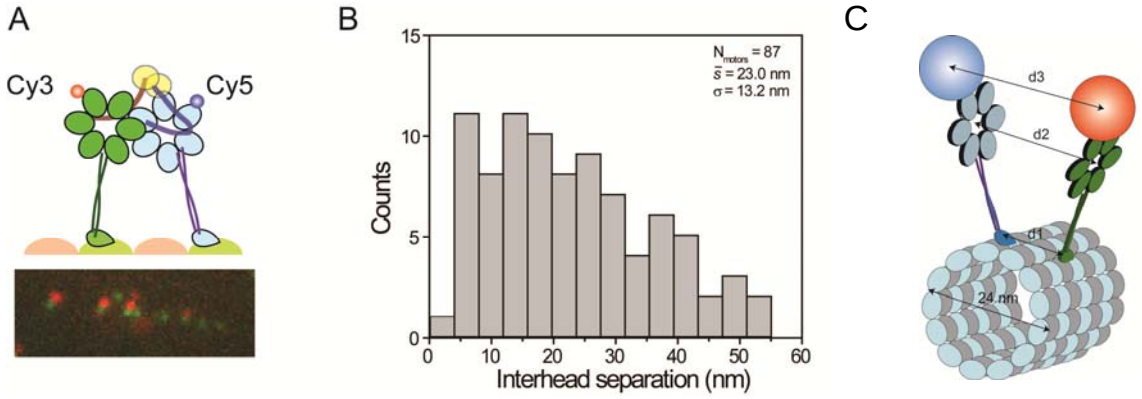

Figure S9. Measurement of the interhead separation using small organic dyes. (**A**) Interhead separation was measured between C-terminal Cy3 and Cy5 dyes on a GST-Dyn_{331kD} construct (top) after immobilizing motors on a microtubule in the apo state (bottom, Cy3: green, Cy5:red). (**B**) The fluorescent images of 87 dual-labeled dynein molecules were analyzed, using the image registration protocol. Mean interhead distance (23.0 ± 13.2 nm) is significantly shorter than the measured distances from QD-labeled dynein dimers (28.4± 10.7 nm, Figure 2A). (**C**) Diagram of a dual QD-labeled dynein on a microtubule shows that the off-axis distance between the two QDs (d_3) overestimates the actual off-axis distance between the heads (d_2) which is also larger than the off-axis distances between the two microtubule binding domains (d_1). This is due to the cylindrical shape of the microtubule filament (24 nm diameter). QD size may not significantly affect the on-axis distance if the heads are oriented parallel to each other and are separated by more than ~12 nm.

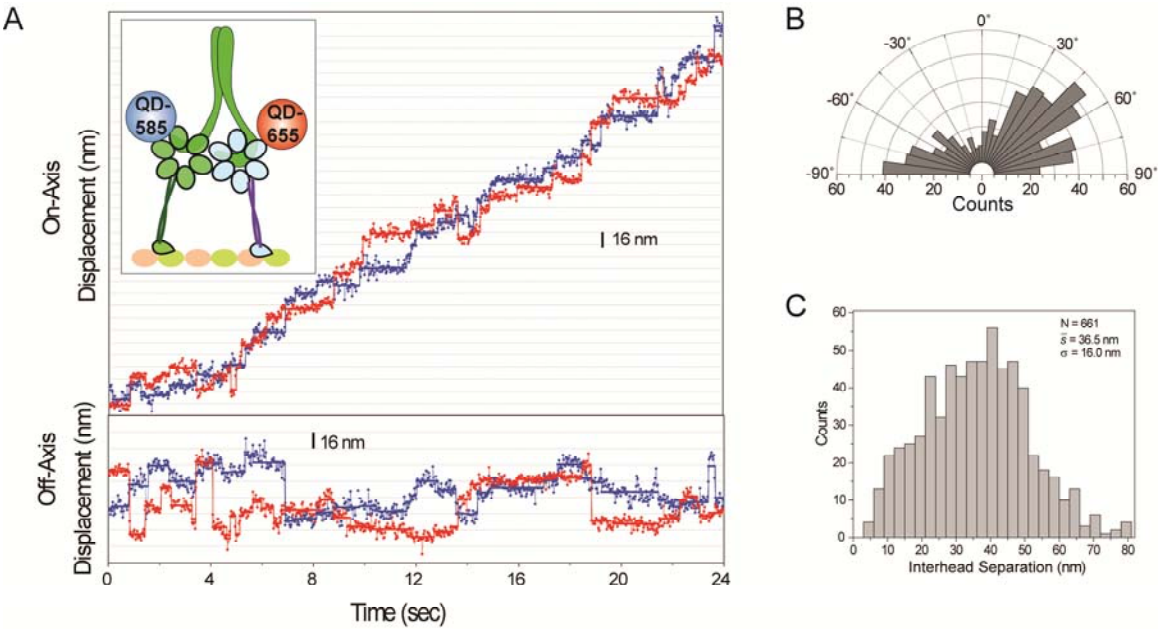

Figure S10. Stepping behavior of a native dynein motor. (**A**) Stepping trace of a native dynein labeled with QD-585 (blue) and QD-655 (red) shows that the heads move independently of each other during processive runs, similar to that of tail-truncated GST-dimer of dynein (GST-Dyn$_{331kD}$). (**B**) Histogram of the angles between the interhead separation vector (from trailing head to the leading head) and microtubule long axis. The leading head prefers to be located on the right hand side relative to the trailing head. (**C**) The heads are separated by 36.5 ± 16.0 nm on average. The average separation of native dynein is larger than that of GST-Dyn$_{331kD}$ (d = 30.4 ± 11.5 nm), possibly due to the larger separation of the heads allowed by the longer linker domain of the native dynein.

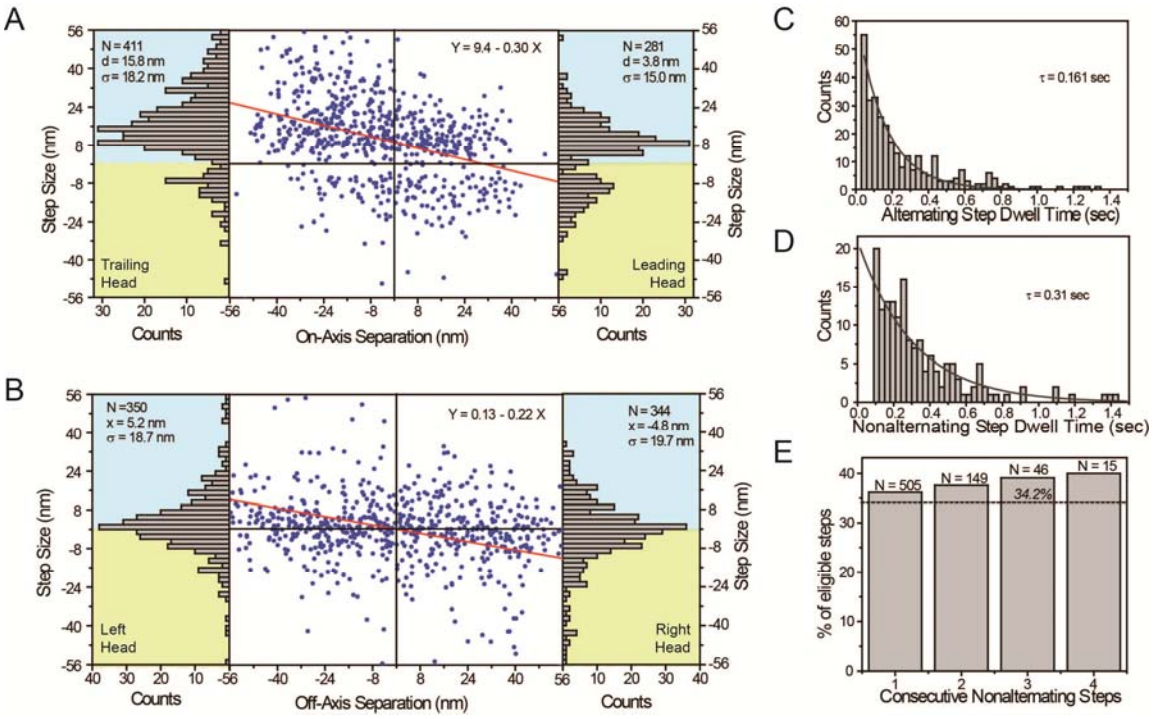

Figure S11. Stepping behavior of native dynein depends on interhead separation, similar to GST-Dyn$_{331kD}$. (**A**) The on-axis step size (blue dots) decreases linearly (red line) as a function of interhead separation and is biased forward by 9.4 ± 0.5 nm. The leading head takes shorter (d = 3.8 nm) steps with more frequent (p_{BW} = 0.34) backward steps, compared to the trailing head (d = 15.8 nm, p_{BW} = 0.16) (bar graphs). (**B**) Off-axis steps show a linear dependence on interhead separation without any bias (0.13 ± 0.53 nm) in the right (positive) or left (negative) directions. On average, the right head takes a ~5 nm step towards the left and *vice versa* (bar graphs). Dependence of the average step size in a native dynein head is less sensitive to interhead separation, compared to GST-Dyn$_{331kD}$ (0.30 vs. 0.38 in on-axis and 0.22 vs. 0.27 in off-axis). This difference may be due to the fact that intramolecular tension between the heads is a function of the length and flexibility of the linker domains. Native dynein, which has a longer linker, may be less sensitive to the extension of the dimer, compared to that of the tail-truncated artificial dimer of GST-Dyn$_{331kD}$. (**C**) Histogram of dwell times between the alternating-head steps of native dynein. Data fits well (R^2 = 0.94) to a single exponential (black line) with a decay constant of 0.161 ± 0.008 sec/step. (**D**) Histogram of dwell times between consecutive steps by the same head (nonalternating steps), before the other head takes a step (exponential decay constant: 0.31 ± 0.03 sec/step, R^2 = 0.83). The ~2-fold difference between the stepping rates of nonalternating and alternating steps favors alternating stepping of the heads. (**E**) The probability of nonalternating stepping, after 0-3 consecutive nonalternating steps remains constant and agrees well with the probability calculated from the decay constants of alternating and nonalternating steps (34.2%)

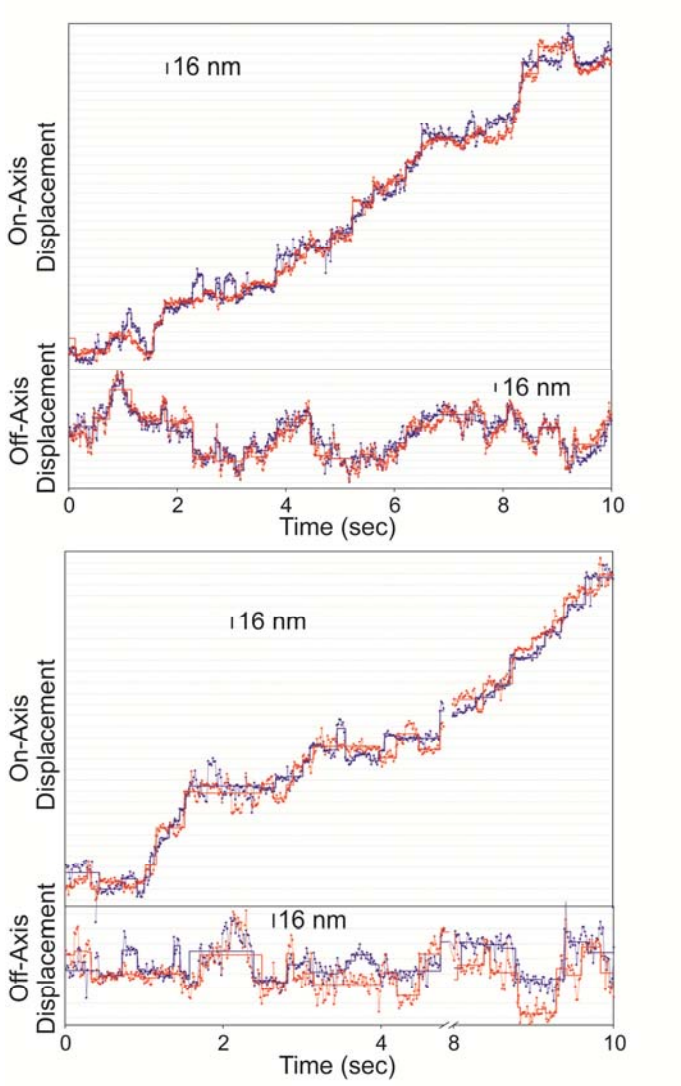

Figure S12. Two additional examples of the stepping motion of the WT_h/Mut_h heterodimer. See Figure 4 and supplemental online methods for details. Bottom traces show sideways stepping along the microtubule off-axis. The raw data is represented by blue (Mut_h) and red (WT_h) dots, while the solid horizontal lines represent steps fitted to the raw data.

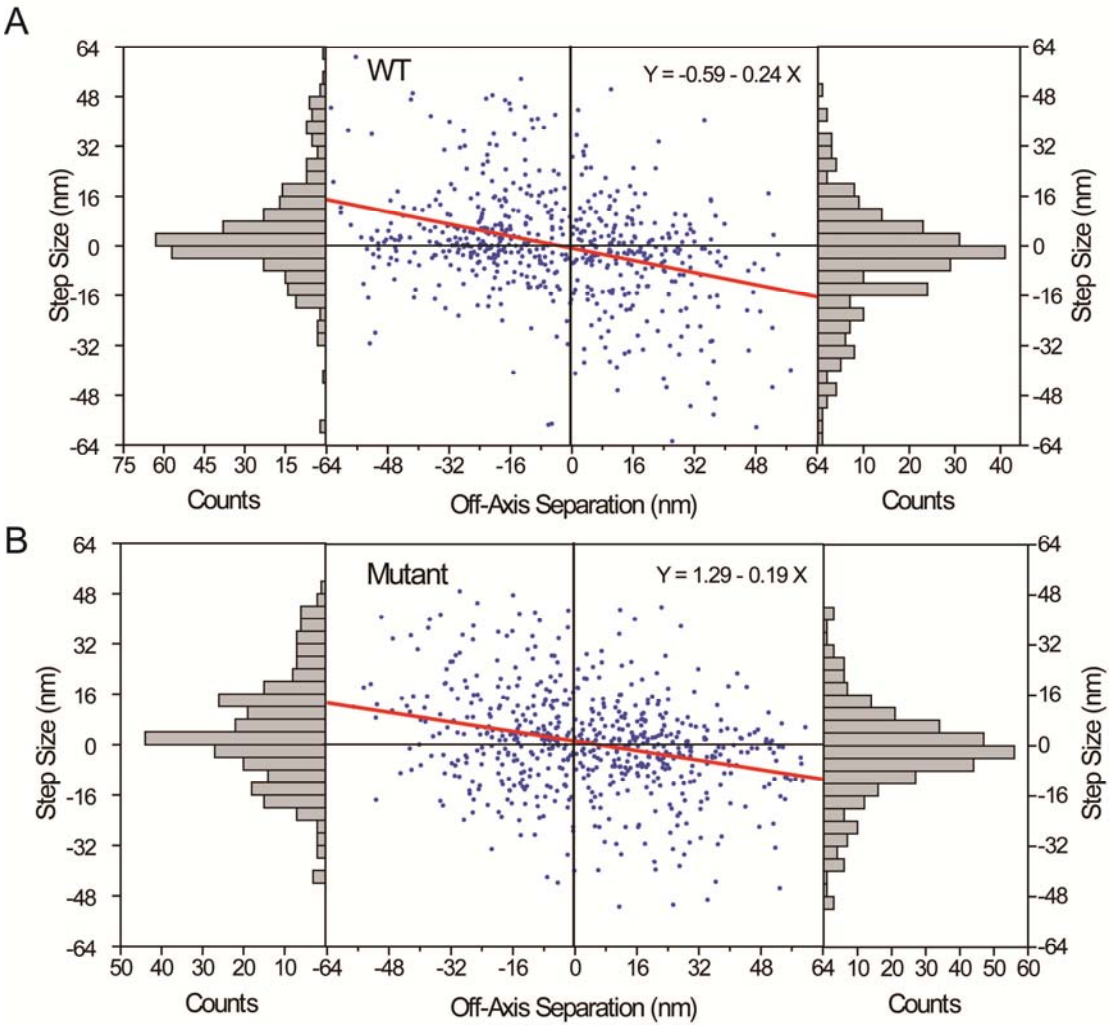

Figure S13. (**A**) Distribution of WT_h off-axis steps as a function of interhead separation. (**B**) Distribution of Mut_h off axis steps as a function of interhead separation. Both heads take frequent sideways steps. However, neither of the two heads has a bias to step towards the left or right directions.

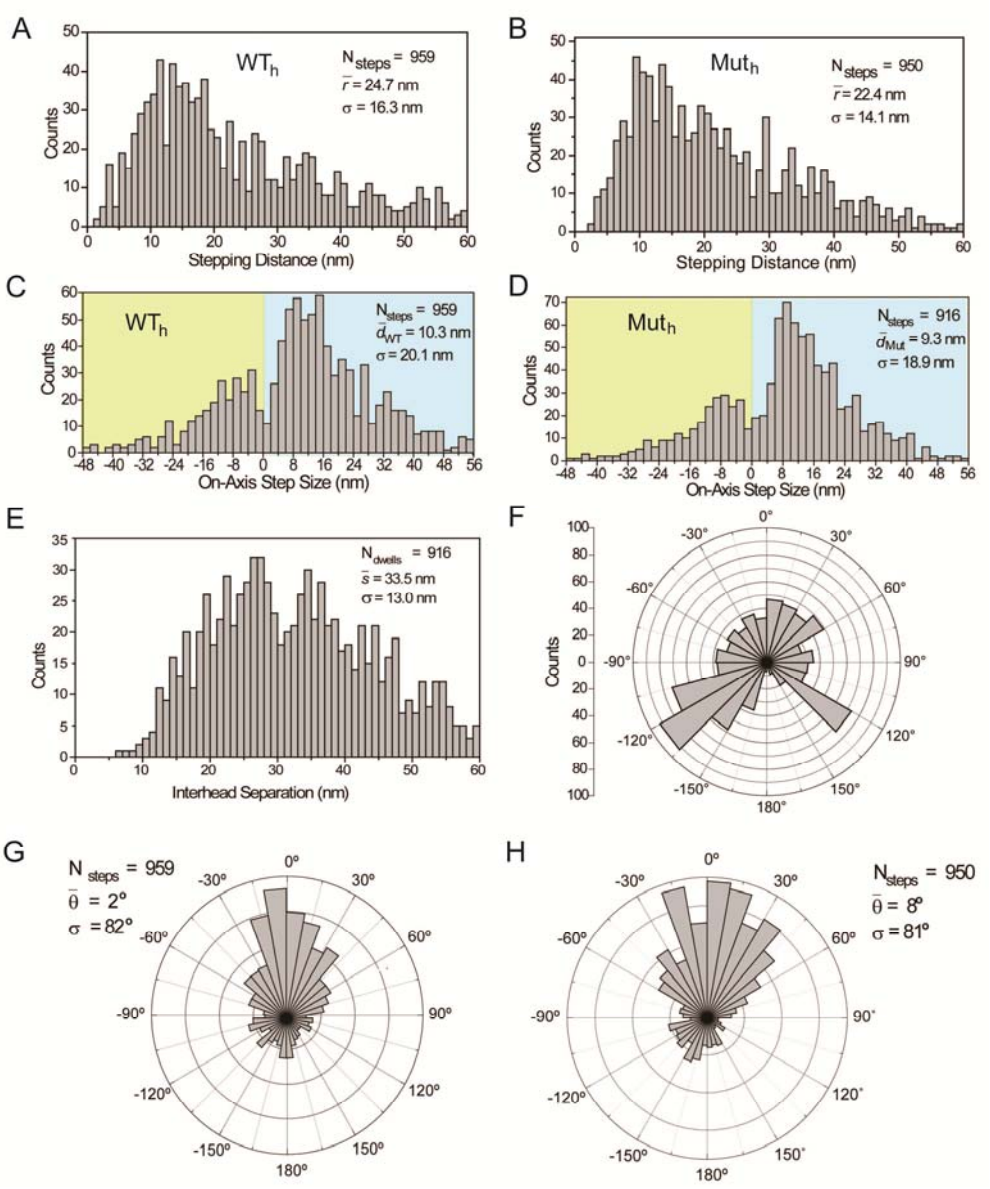

Figure S14. Detailed step size analysis of dual-labeled WT_h/Mut_h heterodimer. (**A-B**) Histograms of the stepping distance of WT_h and Mut_h, respectively. (**C**) On-axis step size histogram of WT_h shows that d_{WT} = 10.3 ± 20.1 nm. (**D**) On-axis step size histogram of Mut_h shows that d_{Mut} = 9.3 ± 18.9 nm. Even though Mut_h has a shorter step size than WT_h both in leading and trailing positions (see Fig. 4), its average step size, d_{Mut}, is only slightly shorter than d_{WT}, because Mut_h trails more often than WT_h. (**E**) Interhead separation between the two heads during dwells (33.5 nm ± 13.0 nm, mean ± st. dev.). (**F**) Angular orientation of Mut_h relative to WT_h shows that Mut_h mostly remains in the trailing position on either the right or left side of WT_h, but it does not prefer to stay right behind WT_h on the same protofilament. (**G**) Histogram of the stepping angles of WT_h with respect to the microtubule minus end. 0° corresponds to an axis parallel to the microtubule minus end. (**H**) Histogram of the stepping angles of Mut_h with respect to the microtubule minus end.

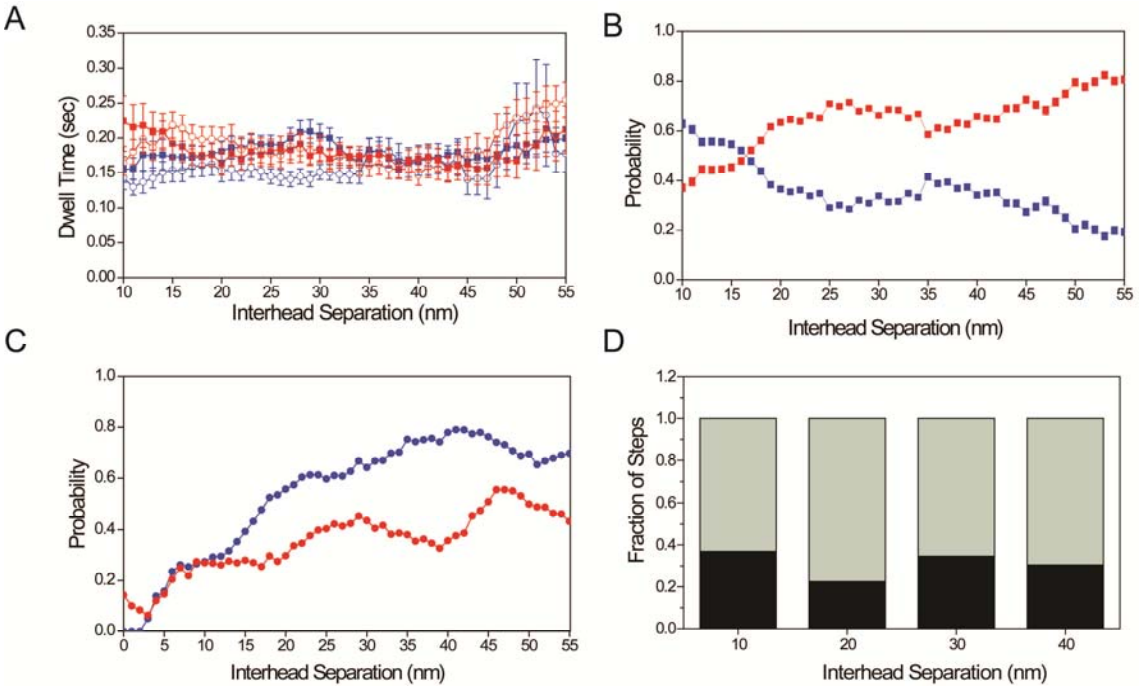

Figure S15. Stepping behavior of the WT_h/Mut_h heterodimer as a function of interhead separation. (**A**) Average dwell time vs. the interhead separation for WT_h (red) and Mut_h (blue), from either the leading (open circles) or trailing (closed squares) positions (10 nm sliding window average). Stepping rates of the two heads remain the same regardless of which head is in the lead. (**B**) The probability of the WT_h (red) and Mut_h (blue) being found in the leading position as a function of interhead separation. (**C**) The probability of the WT_h (red) and Mut_h (blue) taking a step towards the other head as a function of interhead separation. (**D**) Prior to Mut_h moving to the leading position, the fraction of steps taken by Mut_h in the forward direction (light gray) vs. WT_h in the backward direction (black) as a function of interhead separation.

Table S1. Sizes of the QDs used in high resolution tracking assays. The diameter of QDs were measured by dynamic light scattering measurements. Correlograms were fit using Zetasizer instrument software using the "by volume" weighting. See Supplemental Methods for details.

Quantum Dot	**Size (mean ± st.dev.)**
585-NH_2-HaloTag	17.2 ± 1.5 nm
655-NH_2-HaloTag	20.6 ± 4.5 nm
655-Streptavidin	22.1 ± 1.6 nm

Movie S1
Movement of a dual-labeled (green: QD-585, red: QD-655) native homodimeric cytoplasmic dynein motor at 7 μM ATP and 30 msec image acquisition rate. Each pixel is 106 nm.

Movie S2
Animations of the stepping motion of a dynein molecule shown in Movie S1, showing the stepping motion of the QD probes in real time. Blue and red dots represent QD-585 and QD-655 position, respectively.

Movie S3
Movement of a dual-labeled (green: QD-585, red: QD-655) WT_h/Mut_h heterodimeric cytoplasmic dynein motor at 40 μM ATP and 15 msec image acquisition rate. Each pixel is 106 nm.

Movie S4
Animations of the stepping motion of a dynein molecule shown in Movie S3, showing the stepping motion of the QD probes in real time. Blue and red dots represent QD-585 and QD-655 position, respectively.